Study on the Long-Period source mechanism at Campi Flegrei (Italy) by a multi-parametric analysis

E. De Lauro, M. Falanga

Temporary address: Dept. Ingegneria Industriale, Università di Salerno, Via Ponte Don Melillo, 84084 Fisciano (SA), Italy.

S. Petrosino

Istituto Nazionale di Geofisica e Vulcanologia, Sezione di Napoli - Osservatorio Vesuviano, Via Diocleziano 328, Naples 80124, ITALY.

Abstract

The source properties of the Long-Period events that occurred at Campi Flegrei Caldera (Italy) during the 2004-2006 ground uplift episode are investigated by analysing the temporal release of seismic energy, amplitude distribution and inter-event occurrence time. Moreover, an entropy-based decomposition method is applied to identify the "simpler" waveforms thought to be representative of the source mechanism of Long-Period events. On the basis of the outcomes, we propose that the main part of these events is the result of a source process triggered by a mechanism of fluid charge/discharge, which causes pressure drop in a main branch of a dentritic network of the hydrothermal system. In this model, the rate of the Poissonian process (about 15 min), which drives the occurrence of the Long-Period events, provides the average recharge time of the system up to the critical condition. A partial shunting of the fluid flow away from the main conduit activates the "resonance" of a second branch, spatially separated from the first one. This is a process that

occurs whenever the fluid pressure exceeds a critical value and produces less energetic Long-Period events. The mechanism of pressure variation in the two conduits generates signals with preferred amplitude scales, described by a bi-lognormal distribution. From a dynamical point of view, Long-Period events result well described by a low-dimensional dynamical system. Finally, the time pattern of the energy release and its correlation with the diurnal solid earth tide suggest that the whole mechanism of fluid charge/discharge is likely modulated by tidal stress variation.

1. Introduction

The dynamics of the active volcanoes can be described observing their behavior on the many spatial and time scales involved. Indeed, many phenomena may take part in the source process generating complex signals which have to be fully described by means of partial differential equations (infinite degrees of freedom). On the other hand, the coupling between a fluid phase (e.g., magma-gas flow or hydrothermal flux) and the vibrations of the solid (e.g., the volcano edifice) may induce a synchronization mechanism (see for more details, *Pikovsky et al.* [2001]). When the characteristic times of the fluid dynamics match those of the conduit vibrations, spatial coherent oscillations occur, and they can be described by a few degrees of freedom system (see, e.g., *Balmforth et al.* [2005]). In other words, despite the observable complexity, some phenomena like tremor, Long-Period (LP) seismicity and explosion-quakes occurring in volcanic areas may represent a collective behaviour of a low-dimensional dynamical system (see, e.g., *De Lauro et al.* [2008]). The understanding of these source signals not only permits us to

characterize the overall behavior of a volcano and the transition mechanism from a stationary to a non-equilibrium phase, but also provides its specificities.

Useful information is surely obtained by looking at the way in which such active structures release the seismic energy and how this influences the elastic vibrations. This provides some constraints on the charge/discharge process and on the geometry of the solid part. Particularly interesting is the case when the interaction of an aquifer and a magmatic system generates a wide range of phenomena, which can be related to the dynamics of a pressurized subsurface hydrothermal system and to a fluid-rock interaction [*Kumagai and Chouet*, 2000; *Battaglia et al.*, 2006; *Tikku et al.*, 2006; *Gottsmann et al.*, 2007; *Matoza and Chouet*, 2010]. LP events are one of the most common manifestation of this interaction. These signals are characterized by emergent onsets, absence of clear shear wave arrivals and have a typical spectral content in the range 0.2-2 s [see, e.g., *Kawakatsu and Yamamoto*, 2007 and references therein]. Although they frequently occur in active volcanic/hydrothermal areas, few episodes have been recorded at Campi Flegrei volcanic complex [*Saccorotti et al.*, 2001; *Bianco et al.*, 2004]. In particular the most remarkable LP swarm occurred in October 2006 [*Saccorotti et al.*, 2007; *Ciaramella et al.*, 2012] and attracted great attention by the scientific community.

Campi Flegrei volcanic complex is a densely populated area to the West of Naples (Southern Italy). It is a nested caldera originated by two large collapses that occurred during the Campanian Ignimbrite (39 ka) and the Neapolitan Yellow Tuff (NYT; 15 ka) eruptions [*Orsi et al.*, 1996]. The

Campi Flegrei caldera is affected by the phenomenon of bradyseisms, consisting of a slow subsidence alternated with fast ground uplifts. The uplifts are always accompanied by volcano-tectonic (VT) seismicity (high-frequency (>5 Hz) events with clear onsets of compressional and shear wave arrivals, generated by a brittle failure on a fault [*Kawakatsu and Yamamoto*, 2007]). The 2004-2006 deformation episode, despite the small amount of net uplift (5 cm), was accompanied by the largest release of seismic energy ever observed since 1985 [*Saccorotti et al.*, 2007]. A large amount of VT earthquakes (approximately 300 with low-magnitude, M_d <2) occurred between March 2005 and December 2006. Besides VT earthquakes, LP signals were recorded during seven days, starting on October 23, 2006, and with the maximum rate on days 26 and 27. *Saccorotti et al.* [2007] compiled a seismic catalogue that included 338 events, by applying a trigger coincidence criterion to data recorded at two seismic stations (ASB2 and AMS2) with the best signal-to-noise ratio (SNR). These authors observed that about 75% of the detected LPs clusters into three groups of events (clusters 1, 2 and 3) with similar waveform characterized by a correlation coefficient of at least 0.6. The events are located at depths of about 500 m b.s.l. (with errors lower than 100 m) beneath the southern rim of the Solfatara crater: cluster 1 to the West and clusters 2 and 3 to the East, with an approximate distance between the centroids of about 300 m (see, Fig. 1). The LP signals appear like nearly monochromatic oscillations of short duration (<15 s) and frequency content in the band 0.5-2 Hz (Fig. 2). They are ascribed to the acoustic resonance of a crack filled by a water-gas mixture [*Cusano et al.*, 2008], whose hydrothermal origin is also supported by the geochemical observations [*Chiodini et al.*,

2003]. Moreover, *Falanga and Petrosino* [2012] show that LPs are described by a low-dimensional dynamical system and represent self-oscillations generated by a persistent hydrothermal source. At the present, the events detected in October 2006 constitute the most remarkable LP swarm ever recorded in the area, therefore it needs to be studied in detail.

In this paper, we investigate the LPs that occurred at Solfatara volcano looking at the waveform features in terms of cross-correlation and independent component identification. Moreover, we derive their time release of energy and statistical properties including inter-event time mechanism. We also investigate the possible role of longer periodicities such as tidal cycles on the release of energy. The aim is to model in a unique framework the source process of LP seismicity, in terms of a cyclic mechanism of fluid charge/discharge in the conduits of the hydrothermal system, possibly modulated by tidal stress variation.

2. Seismicity and dataset

Data used for the present analysis were collected by five broadband stations (ASB2, AMS2, BGNG, TAGG and OMN2) of the seismic monitoring network of the Campi Flegrei volcanic complex (Fig. 1), managed by the Istituto Nazionale di Geofisica e Vulcanologia-Osservatorio Vesuviano (INGV-OV) and described in details in several recent papers [*Saccorotti et al.*, 2007; *Petrosino et al.*, 2008]. Three-component Lennartz LE-3D/20s seismometers with generator constant G=1000 V/m/s operate at ASB2, AMS2 and OMN2 sites, while stations BGNG and TAGG are equipped with Guralp CMG40T 60s geophones, with generator constant G=800 V/m/s. The sampling rate of

all the digital stations is 125 Hz. We analyze continuous data recorded in the period October 23-29, 2006, corresponding to the LP activity. We focus on the three clusters (138, 30 and 20 events for clusters 1, 2 and 3, respectively) defined by *Saccorotti et al.* [2007], and 152 LPs (orphans) not pertaining to any cluster [*Cusano et al.*, 2008] for a total number of 338 events. In Fig. 2 we show an example of LP waveforms which appear like spindle-shaped signals characterized by emergent onsets.

3. Temporal Energy Release

All the LP events occurred at Solfatara have approximatively the same duration (about 15 s) despite their different amplitudes. In this case, duration-based measures are useless to quantify their energy. On the contrary, such estimate can be obtained by the squared amplitude of a seismic signal, which is proportional to its energy [*Lay and Wallace*, 1995]. We filter all the 338 events in the 0.3-1 Hz frequency band, correct the waveforms for the geometrical spreading and convert the velocity signals into displacement. For each station and each direction of motion, we select a time window of 15 s starting from the signal onset reported in the seismic catalogue [*Saccorotti et al.*, 2007]. Then, we integrated the square of the signal envelope obtained by the Hilbert transform in the selected time window [*De Martino et al.*, 2004]. By plotting these values as a function of time, we obtain the time release of energy (proportional to the squared amplitude) along the investigated period (Fig. 3). This analysis shows evidence that the seismic energy is not equally partitioned among the directions of motion. As for example, the energy estimated for the North-South direction (NS) at ASB2 is higher than

the East-West direction (EW), whereas AMS2 shows an opposite behaviour. The particular large amplitude of the NS with respect to the EW of ASB2 (see also Fig. 2) cannot be explained in terms of possible site effects that could systematically cause ground motion amplification along that particular direction. Indeed, a check was done by comparing the amplitude ratios between the NS and the EW components for the LPs, regional and local VT earthquakes, and the background seismic noise filtered in the 0.3-1 Hz. We find that the average amplitude ratio for the LPs is of a factor 3 greater than that of the other signals. If a strong amplification effect would occur as a site effect, then similar amplitude ratios should have been observed for noise and earthquakes.

Furthermore, the largest amplitudes (and energy release) are observed on NS component of ASB2 and EW component of AMS2 (see also Fig. 2). For these two stations, which depict the best signal-to-noise ratio (SNR), a cross-correlation analysis performed on the LP waveform envelopes also reveals a great degree of similarity between NS component of ASB2 and EW component of AMS2. This holds for all the three clusters and the orphans, although with different percentages. In particular, about the 60% of the LPs of cluster 1 and the 30% for clusters 2, 3 and orphans are correlated over a threshold of 0.8, whereas for any other combination the percentage of correlated waveforms is less than 1%. This is an indication of a repetitive and non-destructive source process (waveform similarities among different directions of motion) with a radial radiation pattern.

After performing the average over the three directions of the retrieved energy, very similar values for all the stations are obtained, as shown in the last

panel of Fig. 3. This suggests that even if energy distributes differently on the three directions of motion, possibly depending on the source-to-station orientation, the total contribution is approximately the same and the results are independent of the station position. Furthermore, the LP amplitude spectra are basically invariant for path correction [*Cusano et al.*, 2008]. Propagation effects due to seismic attenuation affect only the spectral high frequency decay pattern (f >10 Hz), therefore their influence on the signal amplitude can be neglected for these long wavelengths and short distances. Moreover, significant ground motion amplification at low frequency due to site effects is to be excluded on the basis of the results obtained by *Tramelli et al.* [2010]. All these evidences indicate that we are observing a pure source contribution.

3.1. Possible influences on the energy release

The three-component averaged values of the energy span over two orders of magnitude, for the analyzed period. Moreover, although the time series are relatively short, the energy release seems to have a cyclic (quasi-periodic) behaviour with minima and maxima occurring with a nearly diurnal periodicity. To get more insight into this observation, we separate the different clusters of events and plot their distributions in time and energy release. The results, as an example, are shown in Fig. 4 for station ASB2. The cyclic pattern characterizes LPs of cluster 1 and orphans, which occur throughout the whole considered period with both low and high amplitudes. Looking at the distribution in time of cluster 1, it seems the two observed minima and maxima of the energy release both occur in concomitance of the maximum rates of activity. On the contrary, LPs of clusters 2 and 3 occur only in limited time periods (roughly corresponding to night-time), accompanying the

low-amplitude LPs of cluster 1, and are always characterized by a low energy release.

In order to estimate the influence of a possible fluctuation of the noise level on the detection of LPs, we calculate the mean square amplitude of the background signal by using 1-hour-long recordings filtered in the 0.3-1 Hz frequency band, and averaging over the three-directions of motion. In Fig. 4, we observe an increase in the noise level on days 24 and 25 that possibly could have masked the LPs eventually occurred in these days, especially those with low energy. This increase is in coincidence with the gap of the LP temporal distribution (see histograms in the same figure). On the contrary, the noise mean square amplitude is approximately constant and on a low level in the period 26-29 October, when the LP amplitudes are always above the detection threshold defined by the mean level of the noise. Therefore, it seems reasonably that the minima and maxima of the energy release of the LPs are real and not an artefact due to a noisy background that could have prevented the observation of the less energetic events. In other words, a system with energetic levels bounded by a minimum and a maximum is detected during a period when no significative variation of the amplitude of seismic noise occurs. The analysis of the noise amplitude also allows us to exclude possible influences of the anthropogenic sources on the cyclic modulation of the LP energy temporal release. Indeed, a 24 h periodicity could be suspected because of typical of human activities. However, it has been observed that this periodicity generally occurs in the 1-5 Hz frequency band [*Bianco et al.*, 2010], while no periodic behaviour has been observed in the 0.3-1 Hz band, as also confirmed by our results shown in Fig. 4.

Finally, we observe a correlation (0.7) between the LP energy temporal release and the theoretical diurnal solid earth tide generated by the code "solid" (available at the URL http://home.comcast.net/ dmilbert/softs/solid.htm). The maximum of the correlation function corresponds to a time lag of about 9 h, indicating that the two time series are almost in phase opposition (Fig. 4). Low-amplitude cluster 1 LPs, together with LPs of cluster 2 and 3, preferably occur in correspondence of maximum strain, leading to hypothesize that the diurnal periodicity of the LP amplitude distribution could be likely modulated by tidal strain, as we will discuss in Section 7.

4. Amplitude distribution

The occurrence of minima and maxima in the temporal release of the LP energy suggests the existence of a source process which provides different energy levels. To deeply investigate this hypothesis, we calculate the amplitude distribution of all the LPs, considering the average values over the three directions of motion at ASB2. As one can see in the histograms of Fig. 5, the amplitude distribution is bimodal (in logarithmic scale) showing that two preferred energy scales are involved in the generation mechanism. Amplitude distributions showing more than one peak have also been observed, for instance, at Erebus volcano [*De Lauro et al.*, 2009], at Mount St. Helens volcano [*Matoza and Chouet*, 2010] and at Volcàn de Colima [*Zobin et al.*, 2010]. In order to separate the different contributions, we first consider only the clustered LPs. Since the number of events drastically reduces for clusters 2 and 3, the distribution for each of these two families would suffer from data undersampling. This prevents us to make further analysis in order to

discriminate, at a finer level, differences between these two small families. Fig. 5 shows the distributions for all the clusters. As one can note, cluster 1 still retains a bimodal distribution with the main maximum at -6.9 and the second one at -7.3, whereas clusters 2 and 3 are unimodal with a single peak at low energy (-7.3). Therefore, all the LPs belonging to cluster 2 and 3 are events log-normally distributed with a preferred scale in amplitude, and are generally characterized by low-energy. On the contrary, cluster 1 is formed by events with a bimodal amplitude distribution, suggesting that a trigger mechanism providing two preferred values of energy within a broad range has possibly occurred. The preferred scales of energies can be related to different values of the driving pressure. For sake of completeness, we report the amplitude distribution for the orphans, which shows a broader maximum shifted towards the low-amplitude values.

5. Inter-event time analysis

To get an overall understanding of the LP generating process, it is possible to study the macroscopic behaviour taking into account the scale of the occurrence of the events. Indeed, the distribution function of the inter-event times (or inter-times) contains significant information on the dynamic process generating seismic signals [*Bottiglieri et al.*, 2005; *De Lauro et al.*, 2008; 2009]. A qualitative analysis could lead to hypothesize that the occurrence of LPs is a periodic phenomenon. A careful statistical analysis could reveal the existence of significant fluctuations of the inter-times between successive LPs. The inter-event times (Δt) are the differences of the occurrence of two successive LP arrival times [*Cox and Lewis*, 1966]. We focus the attention on

both cluster 1 and orphans; the other clusters suffer too few events making the statistics not significant. For cluster 1 a very clear exponential shape, typical of a Poissonian behaviour [*Cox and Lewis*, 1966], is shown in Fig. 6: the shortest inter-time is the most common of the recurrence time, whereas the longer inter-event times occur with a smaller probability. The fit of the data allows the estimation of the average time interval between LPs $\frac{1}{\lambda} = 14.5$ min, which is the rate of the Poissonian process, i.e., described by an exponential distribution:

$$\phi(\Delta t) = \lambda e^{-\lambda \Delta t}. \tag{1}$$

We perform a standard test to check the Poissonality of the distribution by evaluating the variability coefficient (C_{V1}) defined as $C_{V1} = \frac{\sigma_{\Delta t}}{\overline{\Delta t}}$, where $\sigma_{\Delta t}$ is the standard deviation and $\overline{\Delta t}$ is the mean value of the inter-times. $C_{V1} = 1$ is for a Poissonian process, whereas $C_{V1} > 1$ is for a clustered process and $C_{V1} = 0$ is for a periodic one. The limit $C_{V1} \to \infty$ indicates an uniform distribution. The C_{V1} is equal to 1.0 with an error of 5%, confirming that the occurrence of the LPs is driven by a Poisson process. It is worthwhile to underline that a similar behaviour has been already observed on other volcanoes such as Stromboli [*Bottiglieri et al.*, 2005; *De Lauro et al.*, 2008], Erebus [*De Lauro et al.*, 2009]. A further test to check the hypothesis that the probability distribution function (PDF) for the inter-event times of the LPs is Poissonian is the Kolmogorov-Smirnov (KS) test [*Massey*, 1951]. In the KS test, we assume that the rate parameter λ of the exponential distribution is known and we construct a theoretical exponential cumulative distribution function (TCDF):

$$\Phi(\Delta t) = 1 - e^{-\lambda \Delta t}. \tag{2}$$

The KS test is applied to determine whether the data are distributed according to equation Eq. 2. It is possible to define C_{V2} (the complement of C_{V1}) relative to the distribution in Eq. 2 that in the case of a Poissonian process is *zero*. The KS test statistic is the maximum deviation between the empirical cumulative distribution function (ECDF), calculated from the observed inter-event times, and Φ [*Massey*, 1951; *Rice*, 1995]. The null hypothesis is that the functions are equal. Fig. 6 shows the empirical cumulative distribution function compared with the theoretical one for an exponential distribution. With respect to cluster 1, the optimal value of $\frac{1}{\lambda}$ is 875 s, with KS test passed with a significance level of 0.05; the estimated C_{V2} is nearly zero. The differences are negligible and the strong agreement between the two curves provides a further illustration that the data are well described by an exponential distribution with the estimated rate. This means that the LPs occur randomly in time, but on average one LP occurs approximately every 14.5 min. A similar behaviour is observed for the orphans, which also occur stochastically with an average inter-event time of about 15.3 min.

6. Nonlinear decomposition Analysis: Independent Component Analysis

A non-trivial problem for every experimental time series associated with natural system is to identify individually the degree of complexity of the involved dynamics. There are many powerful methods used for this aim and Independent Components Analysis (ICA) represents a powerful tool [*Hyvärinen et al.*, 2001]. Simulations as well as applications of ICA on real-life data (such as in seismological and acoustic fields) have provided interesting results [*Ac-*

ernese et al., 2003; *De Lauro et al.*, 2007, 2008, 2009]. In its simplest form, ICA performs a blind separation of statistically independent sources, assuming linear mixing of the sources at the sensors on the basis of the intuitive notion of non-Gaussianity. We assume an instantaneous mixing model, thus we neglect any time delay that may occur in the mixing. Formally, the mixing model is written as

$$\mathbf{x}_i = \sum_{j=1}^{n} a_{ij} s_j + \nu \tag{3}$$

where $\mathbf{x}$ is an observed m-dimensional vector (i.e., seismic recordings), $\mathbf{s}$ is an n-dimensional random vector whose components are assumed to be mutually independent; a_{ij} are the constant elements of an $m \times n$ matrix $\mathbf{A}$ to be estimated, and ν is a noise added to the source signal. The additive noise term ν is often omitted in Eq. (3) because it can be incorporated in the sum as one of the independence signals. This mixing is essentially due to path, noise, instrumental transfer functions, etc. In addition to the assumption of independency, we assume that the number of available different mixtures m is at least as large as the number of sources n. Usually, m is assumed to be known in advance, and often $m = n$ thus there exists a probabilistic version of ICA that allows us to by-pass this limit [*Hyvärinen et al.*, 2001]. Only one of the source signals s_i is allowed to have a Gaussian distribution, because it is impossible to separate two or more Gaussian sources [*Bell and Sejnowski*, 1995]. In adaptive source separation an $m \times n$ separating matrix $\mathbf{B}$ is updated so that the vector $\mathbf{y} = \mathbf{B}\mathbf{x}$ is an estimate $\mathbf{y} \simeq \mathbf{s}$ of the original independent source signals.

Some approaches have been proposed in the literature to achieve the separation: maximizing the non-Gaussianity and minimizing the mutual infor-

mation. We remind the reader that the classical measures of non-Gaussianity are the kurtosis and the negentropy J [*Hyvärinen et al.*, 2001]. The latter is less outlier prone than kurtosis. It is based on the information-theoretic quantity of differential entropy H of a random vector $\mathbf{z}$ with density f($\mathbf{z}$) and it is defined as follows:

$$J(\mathbf{z}) = H(\mathbf{z}_{gauss}) - H(\mathbf{z}), \tag{4}$$

where $\mathbf{z}_{gauss}$ is a Gaussian random variable of the same covariance matrix as $\mathbf{z}$. The estimate of negentropy is difficult and, in practice, some approximations must to be introduced. In the following, we shall use the *fixed-point* algorithm, namely FastICA [*Hyvärinen and Oja*, 1997]. Rigorously, this algorithm is based on an approximate Newton iteration scheme.

6.1. Principal Components Analysis

Dimension reduction is a necessary step in the effective analysis of massive data recorded by several stations. They often contain significant redundancies, so one preliminarily investigates if the data-set can be transformed from the high-dimensional space into a fewer dimensional space. Principal Component Analysis (PCA) is well-established and frequently used method for performing a linear mapping of the data to a lower dimensional space in such a way that the variance of the data in the low-dimensional representation is maximized [*Bishop*, 1995; *Hyvärinen et al.*, 2001]. In practise, PCA gives information on the dimensionality of the dynamics that generates the studied signals. With this aim PCA complements ICA giving information on the number of significant independent components to take into account.

Here, we apply PCA to the raw LPs, considering separately all the clusters at each direction of motion. With respect to cluster 1, we observe (Fig. 7) that a few relevant components are representative of the overall dynamics. In particular, we observe that higher amplitude principal components are relative to the polarized ground motion direction: e.g., higher eigenvalues are attained for the EW direction at AMS2 and for the NS at ASB2. At most two representative PCs embed the data (90% of the information content at the knee point) at all stations except for BGNG presumably due to the lower SNR.

With respect to clusters 2 and 3 (Fig. 7) we observe that the low dimensionality of the system is preserved in the sense that generally two components are dominant at the stations with the best SNR (AMS2 and ASB2). Anyway, a greater variability is also evident because of a long tail. This should reflect the difference in the waveforms between the clusters. Because the events of these clusters are lower in energy than cluster 1, the higher amplitude PCs corresponding to the polarized ground motion directions are less evident but still present.

6.2. Independent Components' Identification

PCA provides an indication on the low dimensionality of the clusters and so on the actual number of independent components, in which LPs can be decomposed. Here we apply the ICA to the raw signals in order to extract the related simpler waveforms, considering separately each direction of motion at each different station. In this way, we take into account the cross-correlation analysis, which indicates low correlation among the different directions of motion at the same station. The aim of this analysis it to check whether a

time decomposition is possible and which is the difference among clusters in term of source mechanism.

The seismic records of each LP can be interpreted as a particular linear mixture of some undetermined independent signals. To apply ICA in the linear model mixing we align the traces with respect to the maximum amplitude; the ensuing results are reported in Figs. 8-10. No further decomposition can be accomplished, because ICA performance extracts periodic signals in a background (Gaussian or uniform) noise with an amplitude 1000 times higher than the signal [*De Lauro et al.*, 2005].

Cluster 1 is decomposed into at most three statistically independent components (ICs) (the unknown sources $\mathbf{s}$ of Eq.3), well separated in frequency (Fig. 8). Specifically, we always extract a component in an intermediate frequency range 0.5-0.7Hz (IC2) and a component in the range 0.7-0.9Hz (IC3) at each station but with different amplitudes. In turn, one of each is particular evident on the polarized direction of motion (e.g. IC2 along EW at AMS2 and IC3 along NS at ASB2). Moreover, a very low frequency component centered at 0.2 Hz (IC1) is separated. Furthermore, the performance is good on the horizontal directions; on the vertical direction, instead ICs are generally entangled showing broadband spectra.

Though the greater variability evidenced by PCA, clusters 2 and 3, whose LPs are lower in amplitude, are again decomposed into two independent signals as reported in Figs. 9-10). In details, IC1 is always and better extracted as separate source; it is a stationary signal in the time with a low amplitude in the range 0.1-0.2 mm/s. We can hypothesize that it represents the constant pressure induced by an external source such as micro-meteo marine

noise (wind, oceanic loading) or by an internal source driving the fumarolic system. In order to distinguish between the two cases, it is required to investigate the directional and polarization properties along the time of this wavefield component, but it is beyond the aim of the present paper. IC2 and IC3 are related to LP signals, and extracted according with the polarized directions of motion at each station. For example, focusing the attention on the best SNR stations ASB2 and AMS2, one can see that IC2 is well extracted at AMS2 (in particular along EW) whereas IC3 is extracted at ASB2 (in particular along NS). Furthermore, for cluster 3, ICs are higher in frequency with peaks greater than 1 Hz.

Summarizing, ICA decomposes LPs with regardless of the cluster into at most three ICs in the time domain with very well defined and separate spectral content, indicating a common low-dimensional source mechanism at the basis. This is in agreement with the observations of *Falanga and Petrosino*, [2012] who estimated a correlation dimension of in the range [1.4-1.6] showing evidence that a few degrees of freedom are activated in the system. Focusing the attention on IC2 and IC3, the multiple spectral peaks could be attributed to the presence of different normal modes in the resonating structure [*e.g. Kumagai and Chouet*, 2001], or to the splitting of the stable resonance frequency of the air column in a (thin-walled metal) organ pipe model [*Nederveen and Dalmont*, 2004]. In fact, whenever a wall resonance frequency is close to that of the air column, instabilities occur and the air column oscillations switch between closely spaced frequencies.

We can take into account the following constraints: the differences in the cluster locations are of the order of 300 m (see Fig. 1) [*Saccorotti et al.,*

2007]; no temporal variation in the fundamental frequency and quality factor of LPs is observed [*Cusano et al.*, 2008], suggesting that the likely water-gas mixture involved in the source process does not undergo changes in its composition. We can therefore hypothesize that the clusters can be generated in two (or more) distinct branches of a hydrothermal system, and that their slightly different frequency contents obtained by ICA analysis would be due to different dimensions of the conduits rather than to the variation of the properties of the fluids. This would explain the slightly higher frequencies involved for clusters 2 and 3 compared to 1.

7. Discussion

We have performed a detailed analysis of LP events at Solfatara volcano, Campi Flegrei (Southern Italy). In particular, our study characterizes waveform, spectral and energy properties of the three distinct families of events. Summarizing, the results presented in this work suggest:

1. the three-component averaged energy is of the same order for all the 5 stations used for the analysis;
2. LPs of cluster 1 occur throughout the whole analyzed period with an average inter-event time of about 15 min. The temporal pattern of the energy shows minima and maxima with a diurnal periodicity, and the amplitude distribution is bimodal;
3. the LPs of clusters 2 and 3 principally concentrate during nighttime, and show a single mode distribution peaked on the low values of amplitude;

4. the minima of the temporal energy release of cluster 1 coincide with the occurrences of clusters 2 and 3, whereas the most energetic LPs of cluster 1 are not accompanied by any events of clusters 2 and 3;
5. the temporal and inter-event distributions and energy release of orphan events are similar to those of cluster 1 LPs.
6. PCA and ICA indicate that a very low dimensionality is associated with all the clusters. ICA decomposed the LPs into at most three self-oscillations peaked at about 0.2Hz, 0.5-0.7Hz and 0.7-0.9Hz, which are inferred to be the "resonances" triggered by the hydrothermal fluxes.

These results together suggest that we are observing the actual signature of a source, possibly triggered by a transient pressure disturbance in a fluid medium. Source mechanisms involving harmonic vibrations of cylindrical conduits [*Neuberg et al.*, 2000], acoustic resonance of cracks [*Chouet*, 1988] and non-linear flow-induced oscillations [*Julian*, 1994; *Balmforth et al.*, 2005] have been invoked to explain the LP generation. Independently of the models, the occurrence of a pressure transient in a fluid is the most plausible triggering mechanism [see, e.g., *Hagerty and Benites*, 2003; *Kawakatsu and Yamamoto*, 2007 and reference therein]. The occurrence of LP events with different energies likely depends on the magnitude of the pressure drop in the system [*Chouet et al.*, 1994] and changes in the flow regime may be related to different excitation levels of the system [*Arciniega-Ceballos et al.*, 2003]. Indeed, the amplitude variation of the spectral peaks has been interpreted as different excitations of a common source [*Arciniega-Ceballos et al.*, 2003].

LP events at Campi Flegrei could be originated in a dentritic network of conduits or branches of a hydrothermal system and the deviation of the fluid

flow could explain the dynamics of the observed phenomena. LPs of cluster 1 are produced by the "resonance" of a main structure (compatible with that identified by *Cusano et al.* [2008]) triggered by a pressure transient. The conduit may undergo cycles of gradual sealing, leading to an overpressurization until a critical limit is reached and a consequent discharge of the system occurs. In this model, the inter-event time rate of the Poissonian process (about 15 min) provides the average recharge time of the system up to the critical condition. This nondestructive source process leads to the repetitive waveforms of cluster 1, implying that the trigger mechanisms occur at the same location with the same time function.

A possible (partial) shunting of the fluid flow away from this main conduit reduces the pressure from a maximum value to a minimum level (Fig. 11) and hence only low energy events are generated. The mechanism of pressure variation produces LPs with two preferred amplitude scales, within a certain range. The shunted flux causes a pressure increase in another part of the hydrothermal system and, when it exceeds a critical value (P_{min}; Fig. 11), it activates the "resonance" of the second branch, spatially separated from the main one. This process would originate LPs of clusters 2 and 3, which occur in concomitance of the low energy events of cluster 1. Finally, the orphan events would be triggered by the same prezzurization/depressurization mechanism that produces the clustered LPs, with inter-event time comparable with that of cluster 1 LPs, although in this case the non-repetitive waveforms suggest possible fluctuations of the source location and time function. The important role of the fluids as a source of the dynamics at Campi Flegrei caldera has been recognized by several authors: unrest phases have been explained in

terms of an initial magmatic intrusion from a deep reservoir followed by fluid migration towards the shallow aquifer [*Battaglia et al.*, 2006; *De Natale et al.*, 2006; *Zollo et al.*, 2008; *Chiodini et al.*, 2010]. In that model, ground deformation and LP seismicity represent the response to the pressurization of the hydrothermal system [*De Natale et al.*, 2006; *Cusano et al.*, 2008, *D'Auria et al.*, 2011].

The temporal energy release shows a diurnal modulation not related to the anthropogenic influence, that we ascribe to a tidal effect. It is well known that earth and ocean tides cause deformations in the crust (solid earth) and fluids, therefore tidal stresses can induce fluid flow variations and trigger seismicity [see, e.g., *Glasby and Kasahara*, 2001; *Cochran et al.*, 2004]. Moreover, the correlation between volcanic activity and earth tides has been recognized for a certain number of volcanoes, such as Pavlov, Kilauea, and Arenal [*McNutt and Beaven*, 1981, *Rydelek et al.*, 1988, *Williams-Jones et al.*, 2001, respectively] and in hydrothermal systems [*Jupp and Schultz*, 2004; *Glasby and Kasahara*, 2001 and references therein]. Specifically, some authors have analyzed the relation between tides and seismicity at Campi Flegrei on different time scales from months to days: starting from the seminal paper of *Rydelek et al.* [1992] who found some relations not always fulfilled between the solid-earth tidal stress and triggered earthquakes to *Marzocchi et al.* [2001] who showed evidence of a 24-hour periodicity in the volcano-tectonic earthquake sequence related to thermal diurnal processes. More recently, *De Martino et al.* [2011a, 2011b] at Stromboli volcano have identified a 3-day periodicity transient detected as deformation by the strainmeter and as modulation in the explosion amplitude by the seismometer. This signal reflects a

tidal origin or a possible correlation between earth tides and a phenomenon of non-equilibrium. At Solfatara volcano a similar non-equilibrium condition occurs. This mechanism could modulate fluid flow which in turn determine pressure variation in the pre-existing main branch of the hydrothermal system, thus putting it in oscillation with different energies. The overall effects of such a coupling is the observed diurnal periodicity in the energy temporal release of LP events. In correspondence of the maximum strain, the shunting of the fluid-flow occurs as a pressure drop in the main branch producing lower amplitude LPs, whereas the second branch is simultaneously activated generating the other clusters.

8. Conclusion

The role of fluid migration has been recognized as a fundamental mechanism in the shallow dynamics of Campi Flegrei caldera, as has been pointed out by many authors [*Battaglia et al.*, 2006; *De Natale et al.*, 2006; *Zollo et al.*, 2008; *Cusano et al.*, 2008; *Chiodini et al.*, 2010, *D'Auria et al.*, 2011]. The results presented in this paper fully support this hypothesis; moreover they also indicate a possible tidal effect on the fluids circulating in the geothermal reservoir. Although the shortness of the time series prevented the fine resolution of the periodicities of the tidal constituents, our study shows evidence of a cyclic mechanism of fluid charge/discharge in the branches of the hydrothermal system, which appear to be modulated by tidal stress variation. This mechanism induces pressure drops (mostly in general pressure variations) that can explain the observed time distributions of the LPs and their energy release.

The presented results help to better model at finer scale the LP seismicity that occurred at Campi Flegrei, thus contributing to a better understanding of its source dynamics and the temporal evolution, and putting in place some constraints for the future development of more quantitative models. Future studies need to verify if the hypothesized structures exist and estimate the volume of the source region. Moreover further researches should be aimed at developing a numerical dynamical model including the observed tidal modulation in LP energy release, in order to provide an estimate of the expected amplitude values in case of a new seismic crisis.

In line with these thoughts, a study of the effects of solid earth tides and ocean loading on the modulation of seismic signals recorded over longer time scale will be useful to interpret the dynamics of the shallow hydrothermal system and the unrest episodes of the Campi Flegrei caldera.

9. Acknowledgments

We are sincerely grateful to Dr. Francesca Bianco and Prof. Salvatore De Martino for their useful comments and discussions. The Mobile Seismic Network of the Istituto Nazionale di Geofisica e Vulcanologia, Sezione di Napoli is acknowledged for having collected the data. Dennis Milbert is acknowledged for providing the "solid" code (http://home.comcast.net/ dmilbert/softs/solid.htm). Generic Mapping Tool software has been used to draw the map of Figure 1.

References

[1] Acernese, F., A. Ciaramella, S. De Martino, R. De Rosa, M. Falanga, and R. Tagliaferri, 2003. Neural networks for blind-source separation of Stromboli explosion quakes, IEEE Trans. Neural Networks, 14, 167-175.

[2] Arciniega-Ceballos, A., B. Chouet, and P. Dawson, 2003. Long-period events and tremor at Popocatepetl volcano (1994-2000) and their broadband characteristics, Bull. Volc., 65, 124–135.

[3] Balmforth, E. J., R.V. Craster, and A. C. Rust, 2005. Instability in flow through elastic conduits and volcanic tremor, Journal of Fluid Mechanics, 527, 353-377.

[4] Battaglia, J., C. Troise, F. Obrizzo, F. Pingue, and G. De Natale, 2006. Evidence of fluid migration as the source of deformation at Campi Flegrei caldera (Italy). Geophys. Res. Lett., 33, L01307, doi:10.1029/2005GL024904.

[5] Bell, A. J., and T. J. Sejnowski, 1995. An information-maximisation approach to blind separation and blind deconvolution, Neural Comput., 7, 11291159.

[6] Bianco, F., E. Del Pezzo, G. Saccorotti, and G. Ventura, 2004. The role of hydrotermal fluids in triggering the July-August 2000 seismic swarm at Campi Flegrei, (Italy): evidences from seismological and mesostructural data. J. Volcanol. Geoth. Res., 133, 229–246.

[7] Bianco, F., M. Castellano, R. Cogliano, P. Cusano, E. Del Pezzo, M. A. Di Vito, A. Fodarella, D. Galluzzo, M. La Rocca, G. Milana, S.

Petrosino, S. Pucillo, G. Riccio and A. Rovelli, 2010. Seismic background noise characterization at Campi Flegrei Volcanic Area (Napoli): the "UNREST" Experiment. Quaderni di Geofisica, 86 - Istituto Nazionale di Geofisica e Vulcanologia.

[8] Bishop, C. M., 1995. Neural Networks for Pattern Recognition, Oxford University Press.

[9] Bottiglieri, M., S. De Martino, M. Falanga, C. Godano, and M. Palo, 2005. Europhys. Lett., 72, 493; Research Highlights on Nat. Phys., 1, December issue, (2005).

[10] Ciaramella, A., E. De Lauro, M. Falanga, and S. Petrosino, 2011. Automatic detection of long-period events at Campi Flegrei Caldera (Italy), Geophys. Res. Lett., 38, L18302, doi:10.1029/2011GL049065.

[11] Chiodini, G., M. Todesco, S. Caliro, C. Del Gaudio, G. Macedonio, and M. Russo, 2003. Magma degassing as a trigger of braydseismic events: the case of Phlegrean Fields. Italy. Geophys. Res. Lett., 30(8), 14341438.

[12] Chiodini, G., S. Caliro, C. Cardellini, D. Granieri, R. Avino, A. Baldini, M. Donnini, and C. Minopoli, 2010. Long term variations of the Campi Flegrei (Italy) volcanic system as revealed by the monitoring of hydrothermal activity. J. Geoph. Res., 115, B03205, doi:10.1029/2008JB006258.

[13] Chouet, B.A.,, 1988. Resonance of a fluid-driven crack: radiation properties and implications for the source of long-period events and harmonic tremor. J. Geophys. Res., 93, 4375–4400.

[14] Chouet, B., R. Page, C. Stephens, J. Lahr, J. Power, 1994. Precursory swarms of long-period events a1 Redoubt Volcano, 1989-1990. Alaska: Their origin and use as forecasting tool. J. Volcanol. Geotherm. Res., 62, 95–135.

[15] Cochran, E.S., J.E. Vidale, and S. Tanaka, 2004. Earth tides can trigger shallow thrust fault earthquakes. Science, 306, 1164–1166.

[16] Cox, D. R., and P. A. Lewis, 1966. The statistical analysis of series of events, Metuen, London.

[17] Cusano, P., S. Petrosino, and G. Saccorotti, 2008. Hydrothermal Origin for Sustained Long-Period (LP) activity at Campi Flegrei Volcanic Complex, Italy. J. Volcanol. Geoth. Res., 177, 1035–1044, doi: 10.1016/j.jvolgeores.2008.07.019

[18] D'Auria, L., F. Giudicepietro, I. Aquino, G. Borriello, C. Del Gaudio, D. Lo Bascio, M. Martini, G. P. Ricciardi, P. Ricciolino, and C. Ricco, 2011. Repeated fluid-transfer episodes as a mechanism for the recent dynamics of Campi Flegrei caldera, 1989-2010. J. Geophys. Res., 116, B04313, doi:10.1029/2010JB007837.

[19] De Lauro, E., De Martino, S., Falanga, M., Ciaramella, A., Tagliaferri, R.,, 2005. Complexity of time series associated to dynamical systems inferred from independent component analysis, Phys. Rev. E, 72, 046712(1-14).

[20] De Lauro, E., S. De Martino, M. Falanga, E. Esposito, and E. P. Tomasini, 2007. Analogical model for mechanical vibrations in flue or-

gan pipes inferred by Independent Component Analysis. J. acoust. Soc. Am., 122, 2413–2424, doi:10.1121/1.2772225.

[21] De Lauro, E., S. De Martino, E. Del Pezzo, M. Falanga, M. Palo, and R. Scarpa, 2008. Model for high frequency Strombolian tremor inferred by wavefield decomposition and reconstruction of asymptotic dynamics. J. Geophys. Res., 113, B02302, doi:10.1029/2006JB004838, 393–400.

[22] De Lauro E., S. De Martino, M. Falanga, and M. Palo, 2009. Modelling the macroscopic behavior of Strombolian explosions at Erebus volcano. Phys. Earth Planet. Int., 176, 174–186, doi: 10.1016/j.pepi.2009.05.003.

[23] De Martino, S., M. Falanga and C. Godano, 2004. Dynamical similarity of explosions at Stromboli volcano. Geophys. J. Int., 157, 1247–1254, doi:10.1111/j.1365-246X.2004.02263.x.

[24] De Martino, S., M. Palo, and G. B. Cimini, 2011a. A statistical study of the Stromboli volcano explosion quakes before and during 20022003 eruptive crisis. J. Geophys. Res., 116, B04303, doi:10.1029/2010JB008047.

[25] De Martino, S., M. Falanga, M. Palo, P. Montalto, and D. Patanè, 2011b. Statistical analysis of the volcano seismicity during the 2007 crisis of Stromboli, Italy. J. Geophys. Res., 116, B09312, doi:10.1029/2010JB007503.

[26] De Natale, G., C. Troise, F. Pingue, G. Mastrolorenzo, L. Pappalardo, M. Battaglia, and E. Boschi, 2006. The Campi Flegrei caldera: unrest

mechanisms and hazards. Geological Society, London, Special Publications, 269, 1), 2545, doi: 10.1144/GSL.SP.2006.269.01.03.

[27] Falanga, M., and S. Petrosino, 2012. Inferences on the source of long-period seismicity at Campi Flegrei from polarization analysis and reconstruction of the asymptotic dynamics, Bull. Volcanol., doi:10.1007/s00445-012-0612-2.

[28] Glasby, G.P., and J. Kasahara, 2001. Influence of tidal effects on the periodicity of earthquake activity in diverse geological settings with particular emphasis on submarine hydrothermal systems, Earth-Science Reviews, 52, 261–297.

[29] Gottsmann, J., R. Carniel, N. Coppo, L. Wooller, S. Hautmann, and H. Rymer, 2007. Oscillations in hydrothermal systems as a source of periodic unrest at caldera volcanoes: multiparameter insights from Nisyros, Greece. Geophys. Res. Lett., 34, L07307, doi:10.1029/2007GL029594.

[30] Hagerty, M.T., and R.A. Benites, 2003. Tornillos beneath Tongariro Volcano, New Zealand. J. Volcanol. Geoth. Res., 125(1/2), 151–169.

[31] Hyvärinen, A., and E. Oja, 1997. A Fast Fixed-Point Algorithm for Independent Component Analysis. Neural Comput., 9(7) 1483-1492.

[32] Hyvärinen, A., J. Karhunen, and E. Oja, 2001. Independent Component Analysis, John Wiley & Sons, New York.

[33] Jupp, T. E., and A. Schultz, 2004. A poroelastic model for the tidal modulation of seafloor hydrothermal systems. J. Geophys. Res., 109, B03105, doi:10.1029/2003JB002583.

[34] Julian, B.R., 1994. Volcanic tremor: Nonlinear excitation by fluid flow. J. Geophys. Res., 99, 11859–11877.

[35] Kawakatsu, H., and M. Yamamoto, 2007. Volcano Seismology. In: Schubert G., ed. Treatise on Geophysics Vol. 4. Elsevier, Oxford, 389–420.

[36] Kumagai, H., and B. A. Chouet, 2000. Acoustic properties of a crack containing magmatic or hydrothermal fluids. J. Geophys. Res., 105, 25,49325,512.

[37] Kumagai, H., and B. A. Chouet, 2001. The dependence of acoustic properties of a crack on the resonance mode and geometry. Geophys. Res. Lett., 28(17), 33253328.

[38] Lay, T., and T. C. Wallace (1995). Modern Global Seismology, Academic Press, London.

[39] Marzocchi, W., G. Vilardo, D.P. Hill, G.P. Ricciardi, and C. Ricco, 2001. Common features and peculiarities of the seismic activity at Phlegraean fields, Long Valley and Vesuvius, Bull. Seismol. Soc. Am., 91, 191205.

[40] Massey, F. J., 1951. The Kolmogorov-Smirnov test for goodness of fit. J. Am. Stat. Assoc., 46, 68–78.

[41] Matoza, R. S., and B. A. Chouet, 2010. Subevents of long-period seismicity: Implications for hydrothermal dynamics during the 2004-2008 eruption of Mount St. Helens.J. Geophys. Res., 115, B12206, doi:10.1029/2010JB007839.

[42] McNutt, S. R., and R. J. Beavan, 1981. Volcanic earthquakes at Pavlof volcano correlated with the solid earth tide, Nature, 294, 615618.

[43] Nederveen, C. J., and J. P. Dalmont, 2004. Pitch and level changes in organ pipes due to wall resonances. Journal of Sound and Vibration, 271, 227–239.

[44] Neuberg, J., R. Luckett, B. Baptie, and K. Olsen, 2000. Models of tremor and low-frequency earthquake swarms on Montserrat. J. Volcanol. Geoth. Res., 101, 83-104.

[45] Orsi, G., S. De Vita, and M.A. Di Vito, 1996. The restless resurgent Campi Flegrei nested caldera, Italy): constraints on its evolution and configuration. J. Volcanol. Geoth. Res., 74, 179–214.

[46] Petrosino, S., L. De Siena, and E. Del Pezzo, 2008. Recalibration of the Magnitude Scales at Campi Flegrei, Italy, on the Basis of Measured Path and Site and Transfer Functions. Bull. Seism. Soc. Am., 98(4), 1964–1974.

[47] Pikovsky, A., M. Rosenblum, and J. Kurths, 2001. SYNCHRONIZATION, A Universal Concept in Nonlinear Sciences, Cambridge University Press.

[48] Rice, J. A., 1995. Mathematical Statistics and Data Analysis, 2nd ed., Duxbury, Belmont, Calif.

[49] Rydelek, P., P. Davis, and R. Koyanagi, 1988. Tidal Triggering of Earthquake Swarms at Kilauea Volcano, Hawaii. J. Geophys. Res., 93(B5), 4401-4411.

[50] Rydelek, P.A., I.S. Sacks, and R. Scarpa, 1992. On tidal triggering of earthquakes at Campi Flegrei, Italy. Geophys. J. Int., 109, 125137.

[51] Saccorotti, G., F. Bianco, M. Castellano, and E. Del Pezzo, 2001. The July-August 2000 seismic swarms at Campi Flegrei volcanic complex, Italy. Geophys. Res. Lett., 28, 2525–2528.

[52] Saccorotti, G., S. Petrosino, F. Bianco, M. Castellano, D. Galluzzo, M. La Rocca, E. Del Pezzo, L. Zaccarelli, and P. Cusano, 2007. Seismicity associated with the 2004-2006 renewed ground uplift at Campi Flegrei Caldera, Italy. Phys. Earth Planet. Inter., 165, 14–24.

[53] Tikku, A. A., D. C. McAdoo, M. S. Schenewerk, and E. C. Willoughby, 2006. Temporal fluctuations ofmicroseismic noise in Yellowstone's Upper Geyser Basin from a continuous gravity observation. Geophys. Res. Lett., 33, L11306, doi:10.1029/2006GL026113.

[54] Tramelli, A., D. Galluzzo, E. Del Pezzo, and M. A. Di Vito, 2010. A detailed study of the site effects in the volcanic area of Campi Flegrei using empirical approaches. Geophys. J. Int., 182, 10731086, doi: 10.1111/j.1365-246X.2010.04675.x.

[55] Williams-Jones, G., J. Stix, M. Heiligmann, J. Barquero, E. Fernadez, and E.D. Gonzalez, 2001. A model of degassing and seismicity at Arenal Volcano, Costa Rica. J. Volcanol. Geotherm. Res., 108, 121139.

[56] Zobin, V. M., O. E. Melnik, M., González, O., Macedo, and M. Bretón, 2010. Swarms of microearthquakes associated with the 2005 Vulcanian

explosion sequence at Volcn de Colima, Mxico. Geophys. J. Int., 182, 808828. doi: 10.1111/j.1365-246X.2010.04647.x.

[57] Zollo, A., N. Maercklin, M. Vassallo, D. Dello Iacono, J. Virieux, and P. Gasparini, 2008. Seismic reflections reveal a massive melt layer feeding Campi Flegrei caldera. Geophys. Res. Lett., 35, L12306, doi:10.1029/2008GL034242.

Figure 1: Map of the Campi Flegrei area with the seismic stations used for the present analysis (triangles). The location of LPs of cluster 1 (black circles), cluster 2 (blue circles) and cluster 3 (red circles) in the Solfatara are also shown (after *Saccorotti et al.* [2007]).

Figure 2: Example of seismograms of a LP recorded on 26 October 2006. The station name and the direction of motion are indicated in the upper-left corner of each plot.

Figure 3: Temporal release of seismic energy (proportional to the squared amplitude) for the three directions of motion at the different stations. In the last panel the average value of the energy over the three components is reported.

Figure 4: Temporal release of seismic energy, proportional to the squared amplitude (open circles, triangles, squares and diamonds), and time distribution (histograms) for clusters 1, 2, 3 and orphans (see symbol legend) at ASB2 station. Purple and yellow full circles represent the square amplitude of the seismic noise averaged over 1-hour-long recordings, filtered in the 0.3-1 Hz and 1-5 Hz frequency band, respectively. The magenta continuous line is the theoretical solid earth tide.

Figure 5: Amplitude distribution for all the LPs; LPs of cluster 1; LPs of cluster 2 plus 3; and orphans.

Figure 6: Inter-time analysis for LPs of cluster 1 (black) and for the orphans (green): (A) distribution of the inter-times; (B) linear best fit providing the characteristic rate of the Poissonian process; (C) comparison between ECDF (solid line) and TCDF (dots) according to the KS test with the estimated rates; (D) residuals between ECDF and TCDF are negligible in agreement with the hypothesis of Poissonality.

Figure 7: PCA results: the overall dynamics for all clusters is essentially low dimensional. In detail, for cluster 1 at most two PCs retain the maximum information content. For cluster 2 and cluster 3 the two PCs are still dominant even if the stations with lower SNR (TAGG and BGNG) show a greater variability. In addition, it is clearly shown that the higher amplitude PCs are relative to the polarized ground motion direction for all the clusters.

Figure 8: ICA results for cluster 1 at each direction of motion for AMS2 and ASB2. The decomposition provides at most three "simpler" waveforms thought to be representative of the source mechanism of long-period earthquakes.

Figure 9: ICA results for cluster 2 at each direction of motion for AMS2 and ASB2: the data are well described by a low-dimensionality system and that the seismic cluster 2 can be decomposed into two independent components.

Figure 10: ICA results for cluster 3 at each direction of motion for AMS2 and ASB2: the system is still low-dimensional, but the extracted signals display a slightly higher frequency content.

Figure 11: Conceptual model for the LPs generation mechanism. The shunting of the fluid flow between the two branches of the hydrothermal system causes a pressure drop in the conduit A and activates the resonances of the conduit B (lower panel). As a consequence, the pressure P_A in the branch A varies from a maximum to a minimum level, triggering LPs of cluster 1 with different amplitude. Moreover, when P_B exceeds the minimum threshold value P_{min}, LPs of clusters 2 and 3 are generated in the branch B (upper panel).

Figure(s)
Click here to download Figure(s): fig1.eps

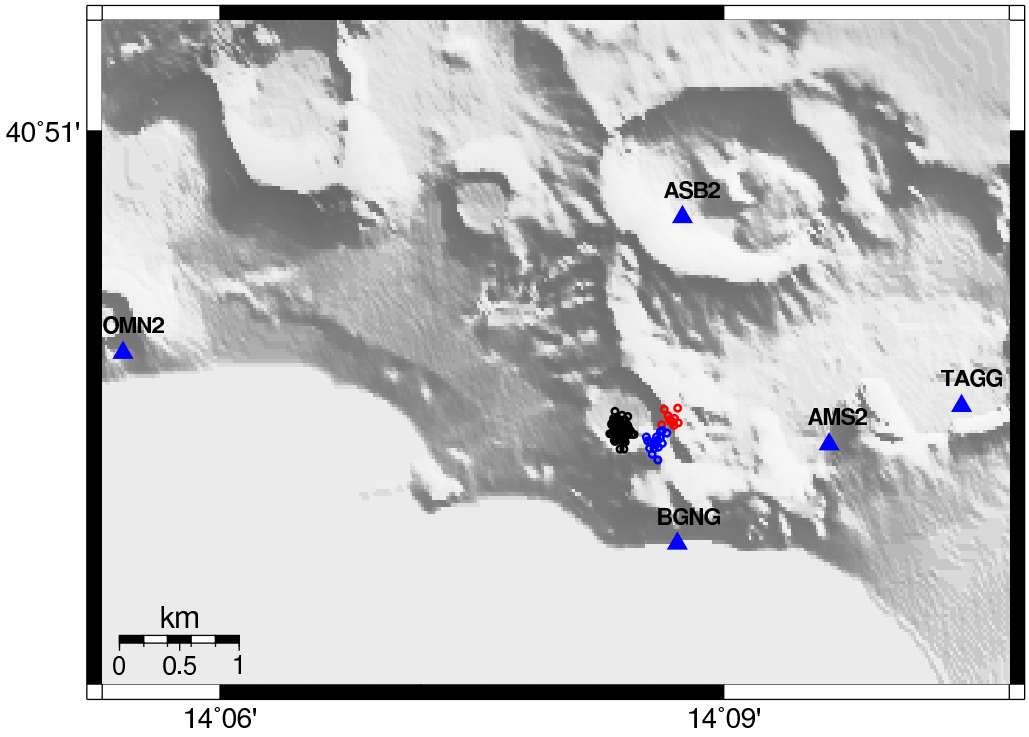

Figure(s)

Click here to download Figure(s): fig2.pdf

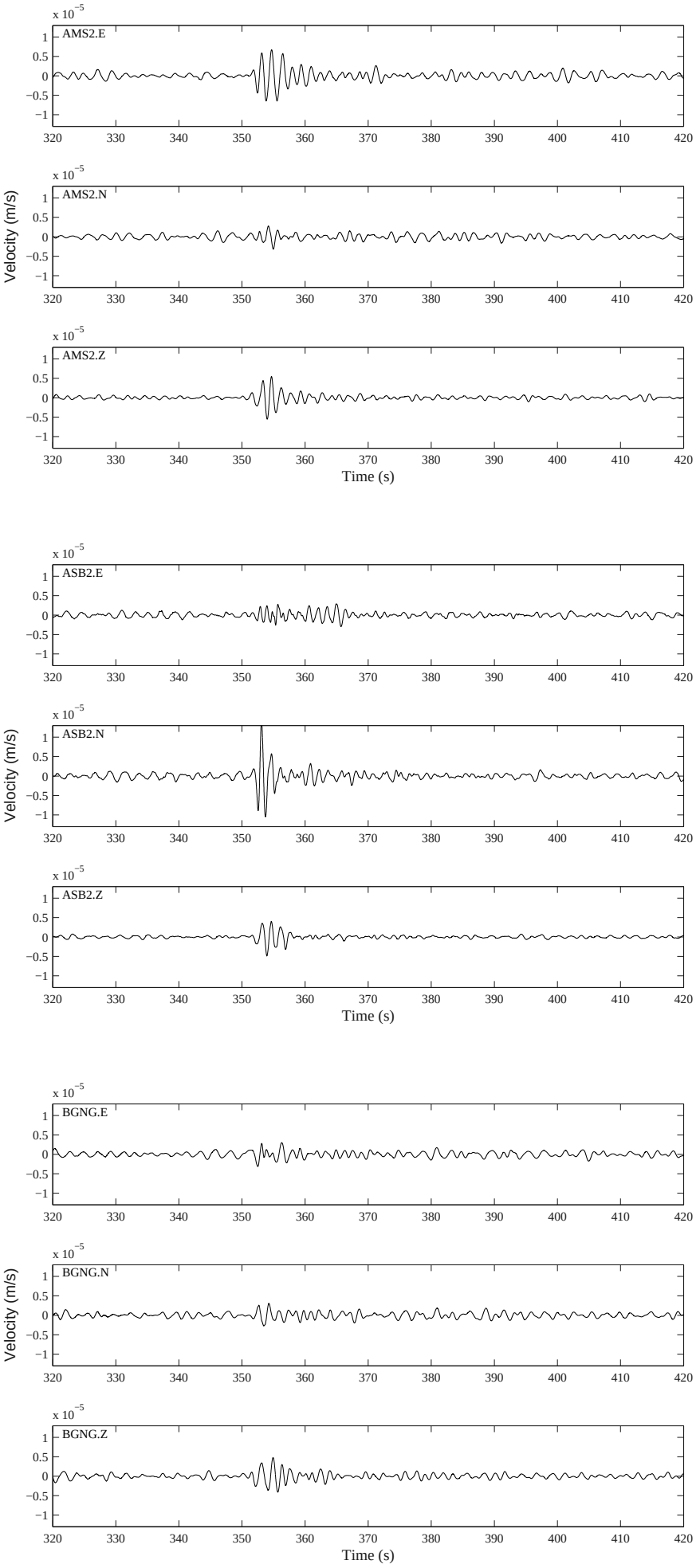

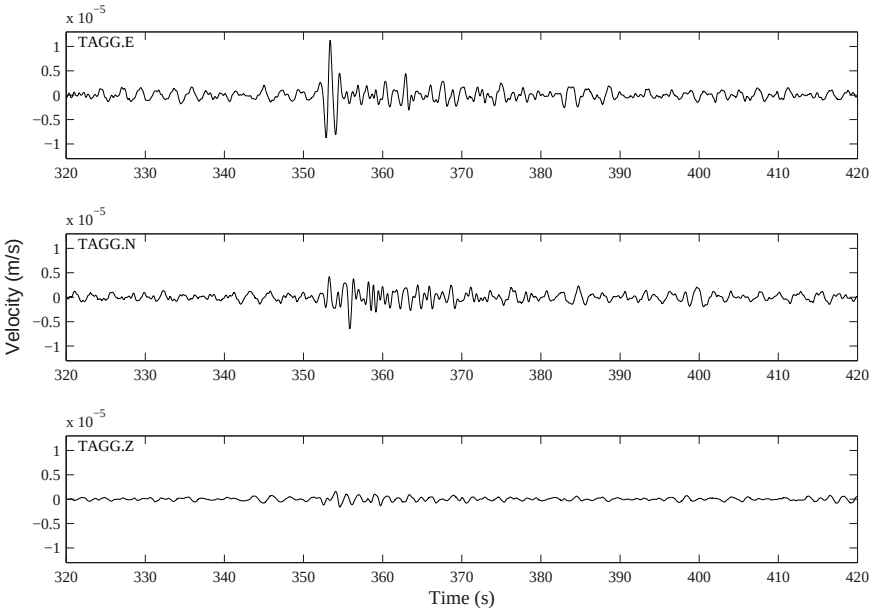
x 10^−5
TAGG.E
TAGG.N
TAGG.Z
Velocity (m/s)
Time (s)

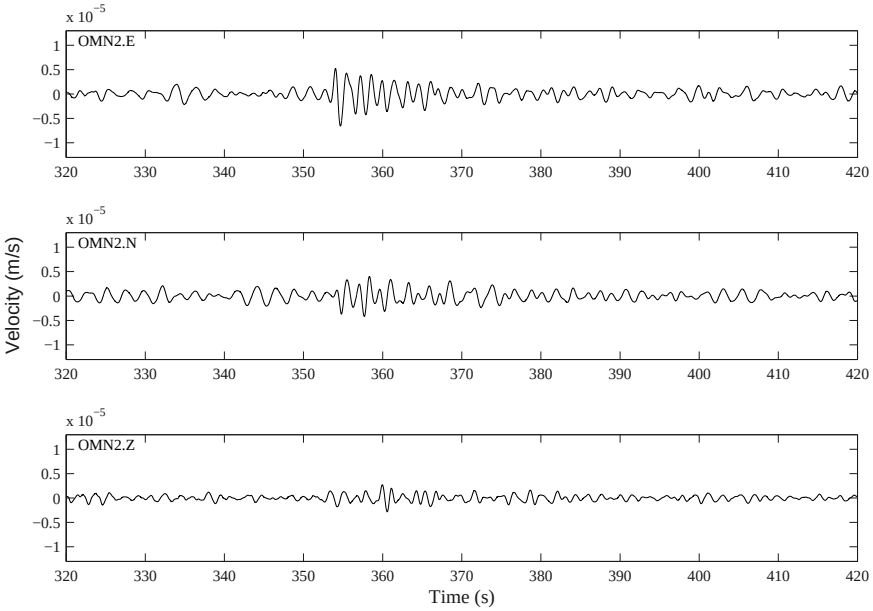
x 10^−5
OMN2.E
OMN2.N
OMN2.Z
Velocity (m/s)
Time (s)

Figure(s)

Click here to download Figure(s): fig3.eps

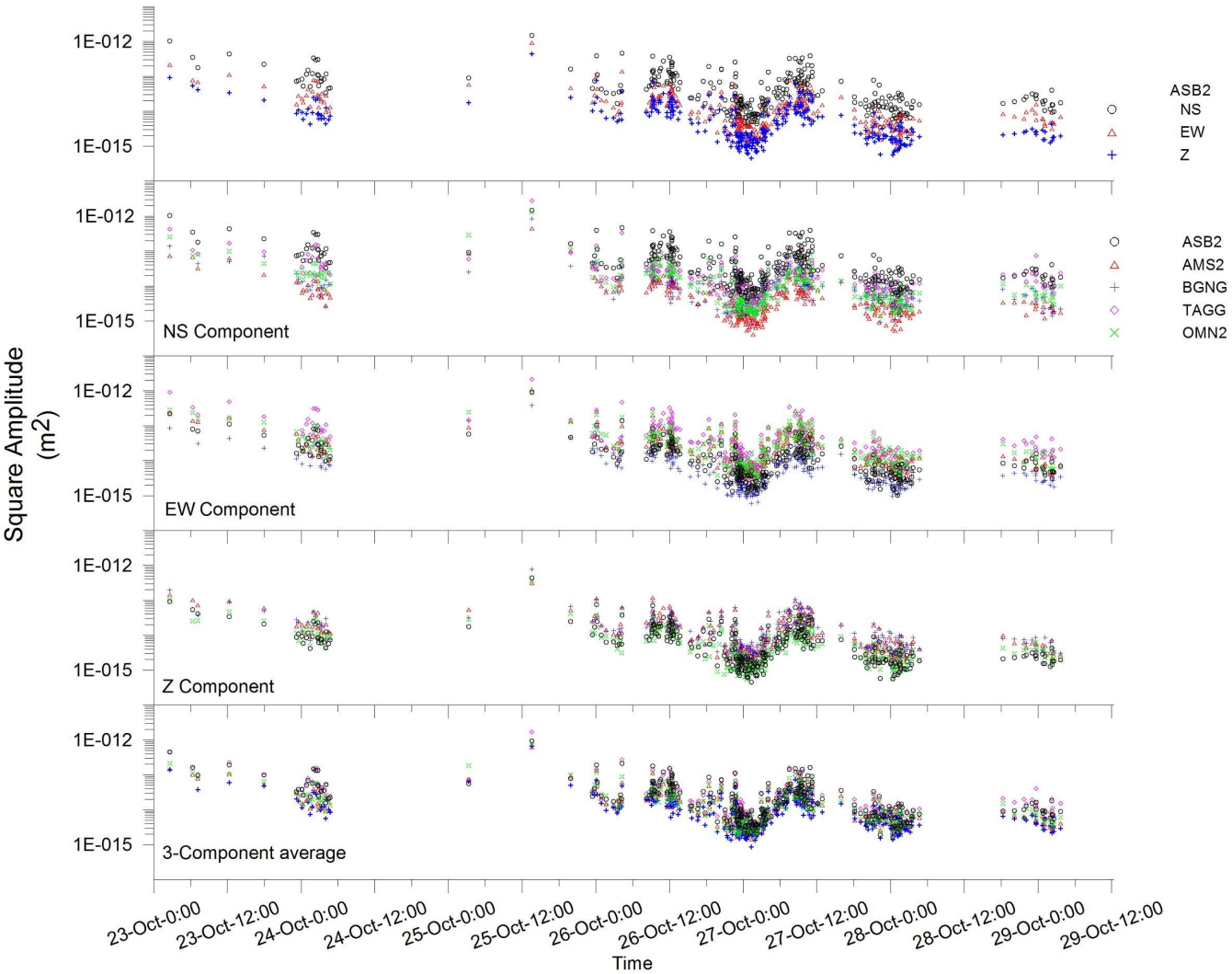

Figure(s)

Click here to download Figure(s): fig4.eps

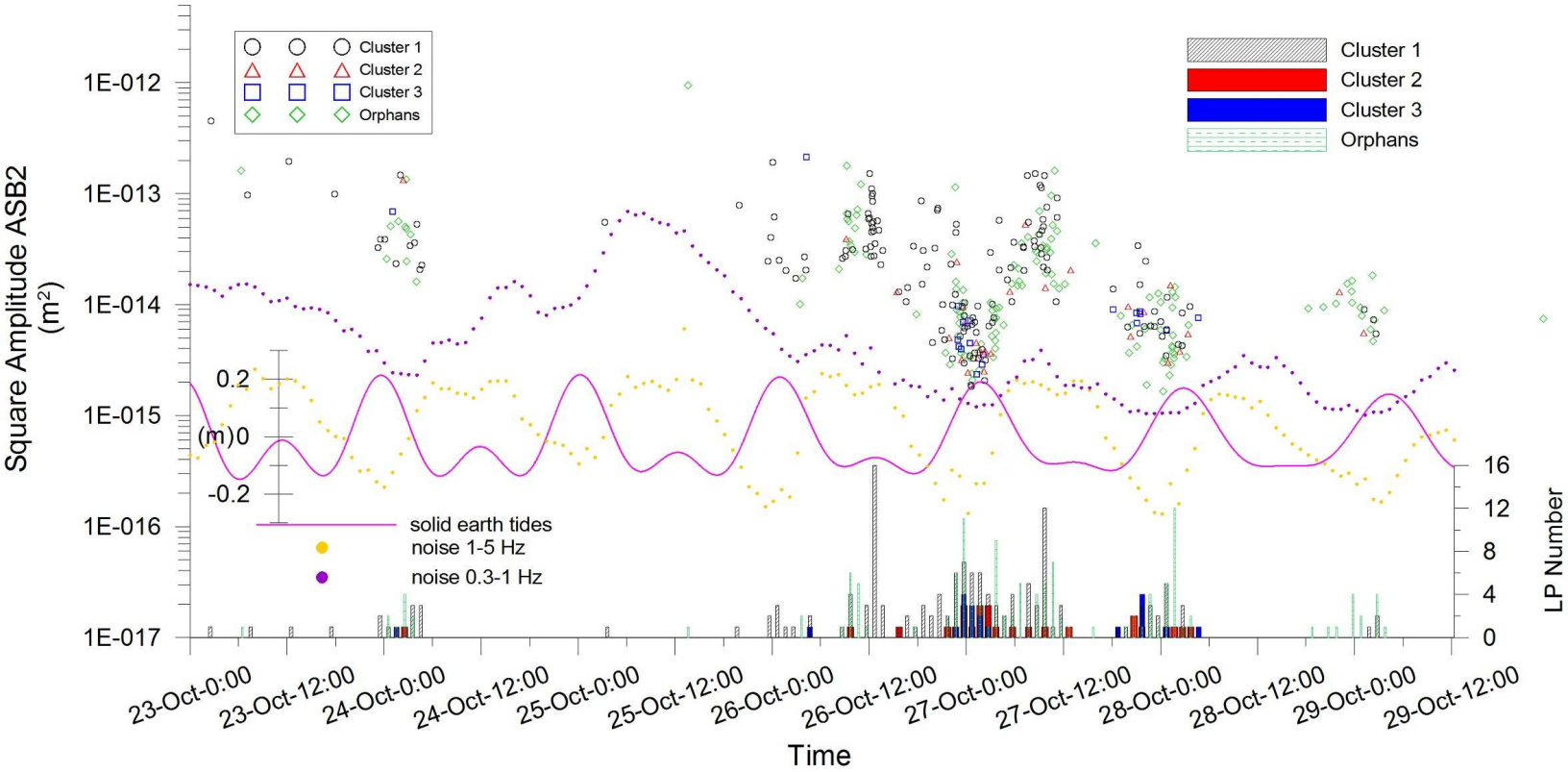

Figure(s)
Click here to download Figure(s): fig5.eps

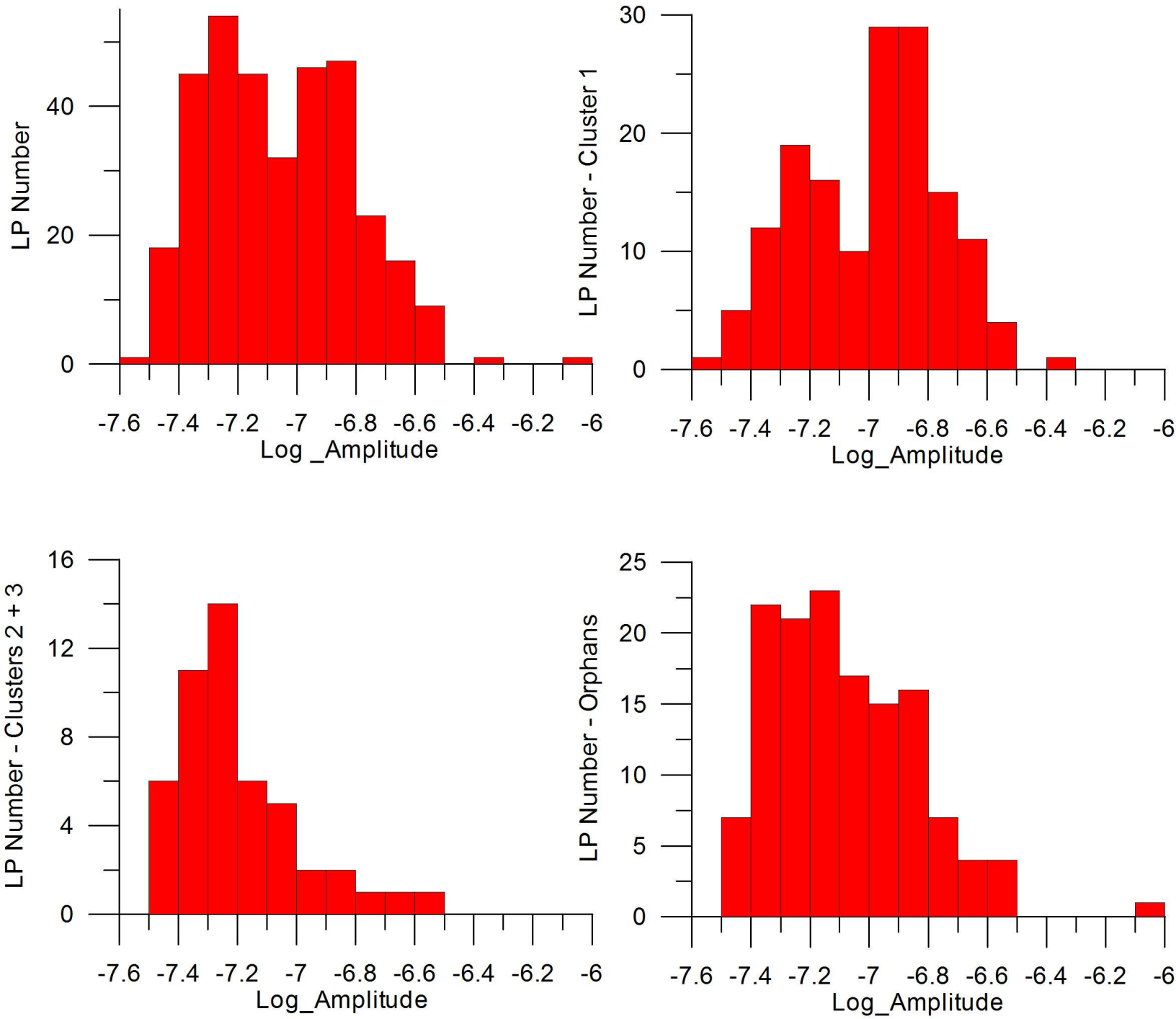

Figure(s)
Click here to download Figure(s): fig6.eps

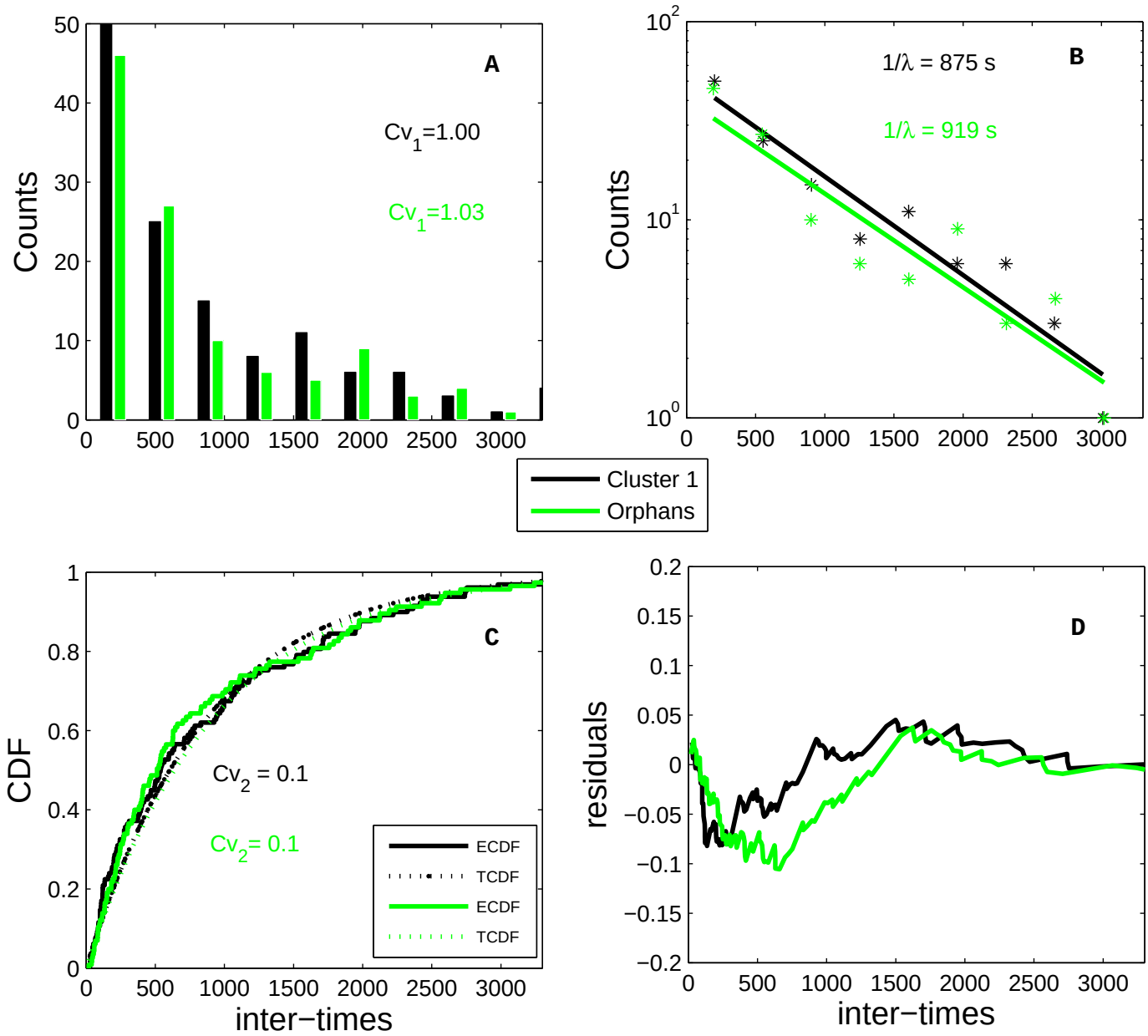

Figure(s)
Click here to download Figure(s): fig7.eps

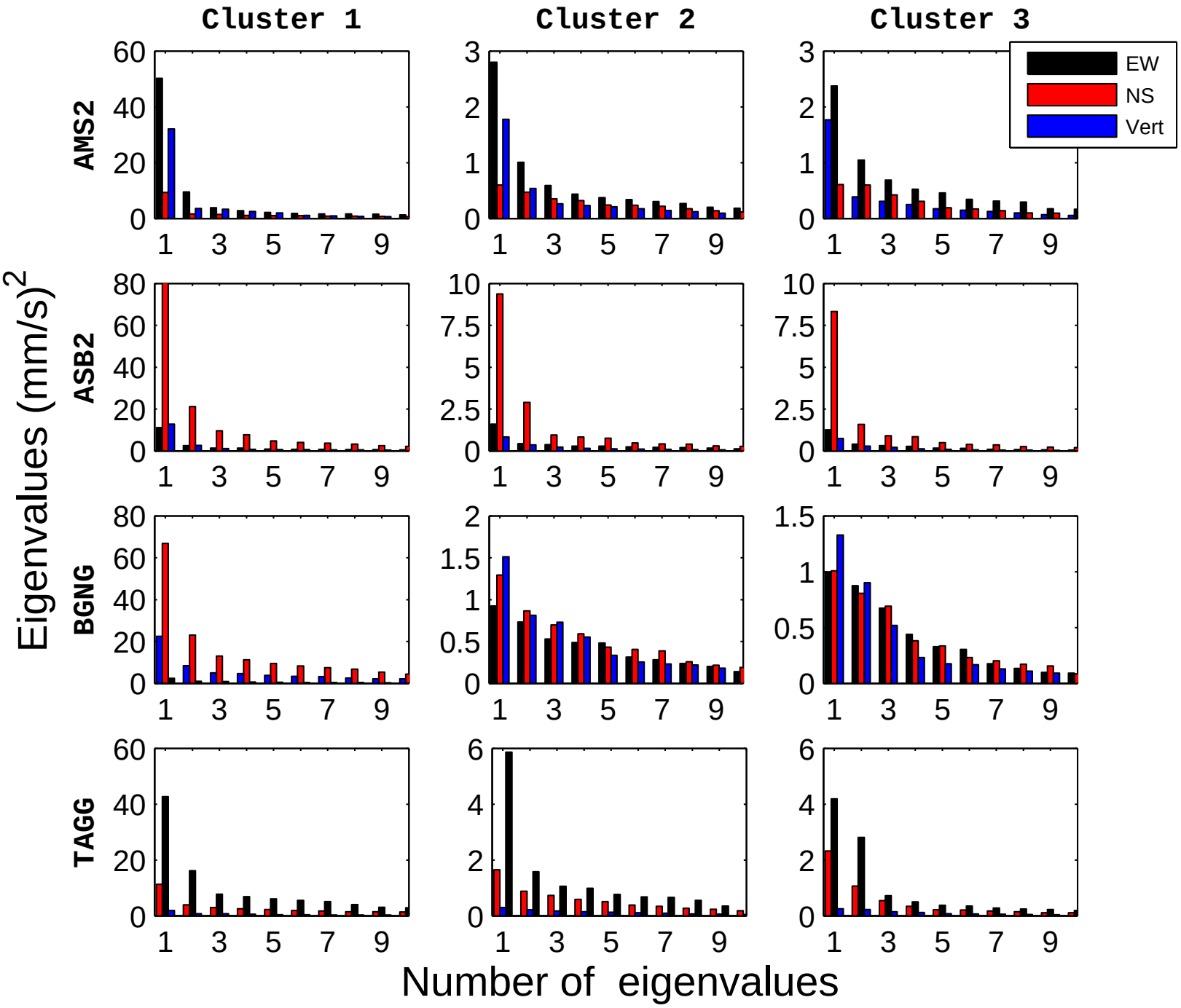

Figure(s)

Click here to download Figure(s): fig8.eps

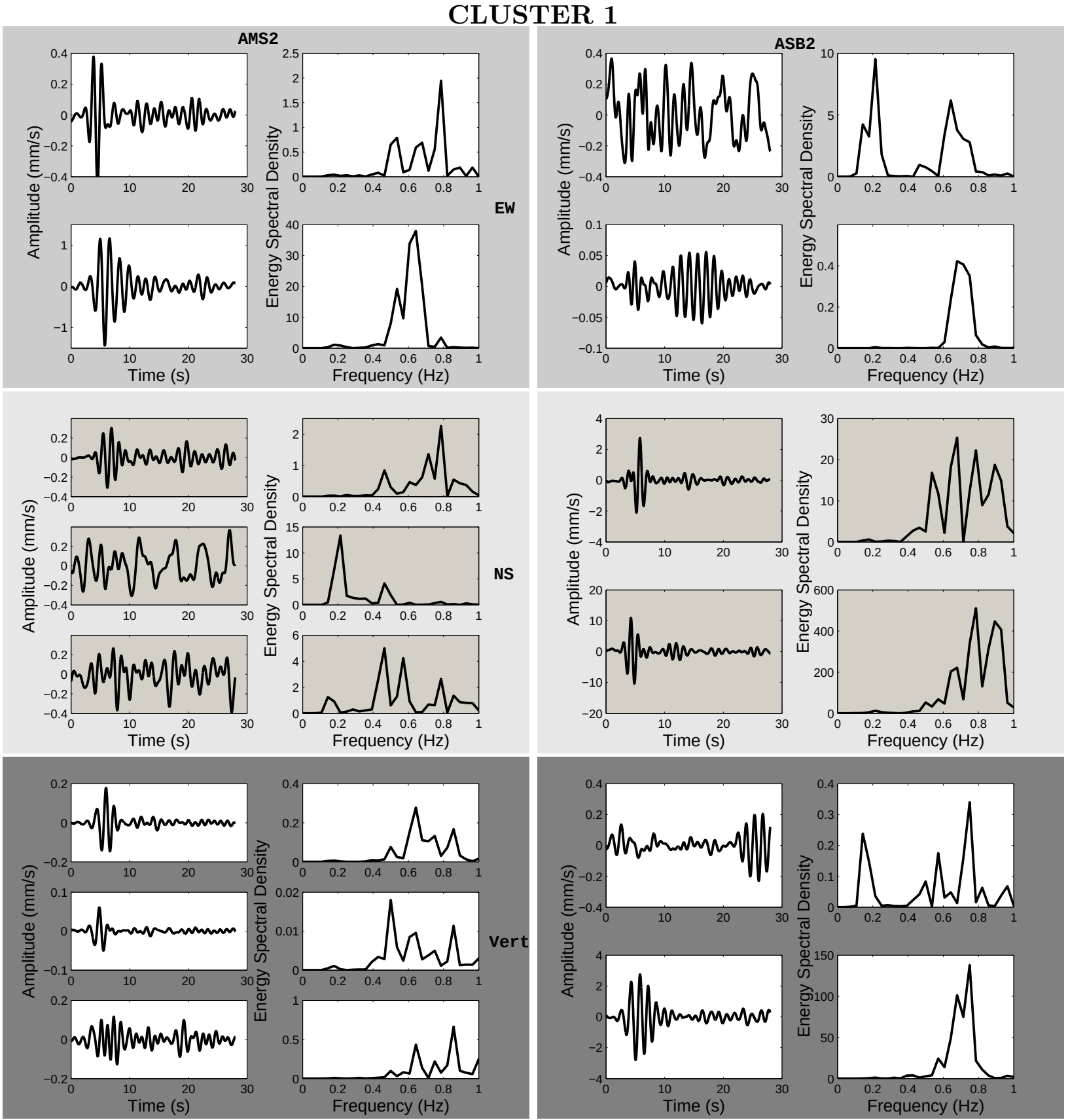

Figure(s)

Click here to download Figure(s): fig9.eps

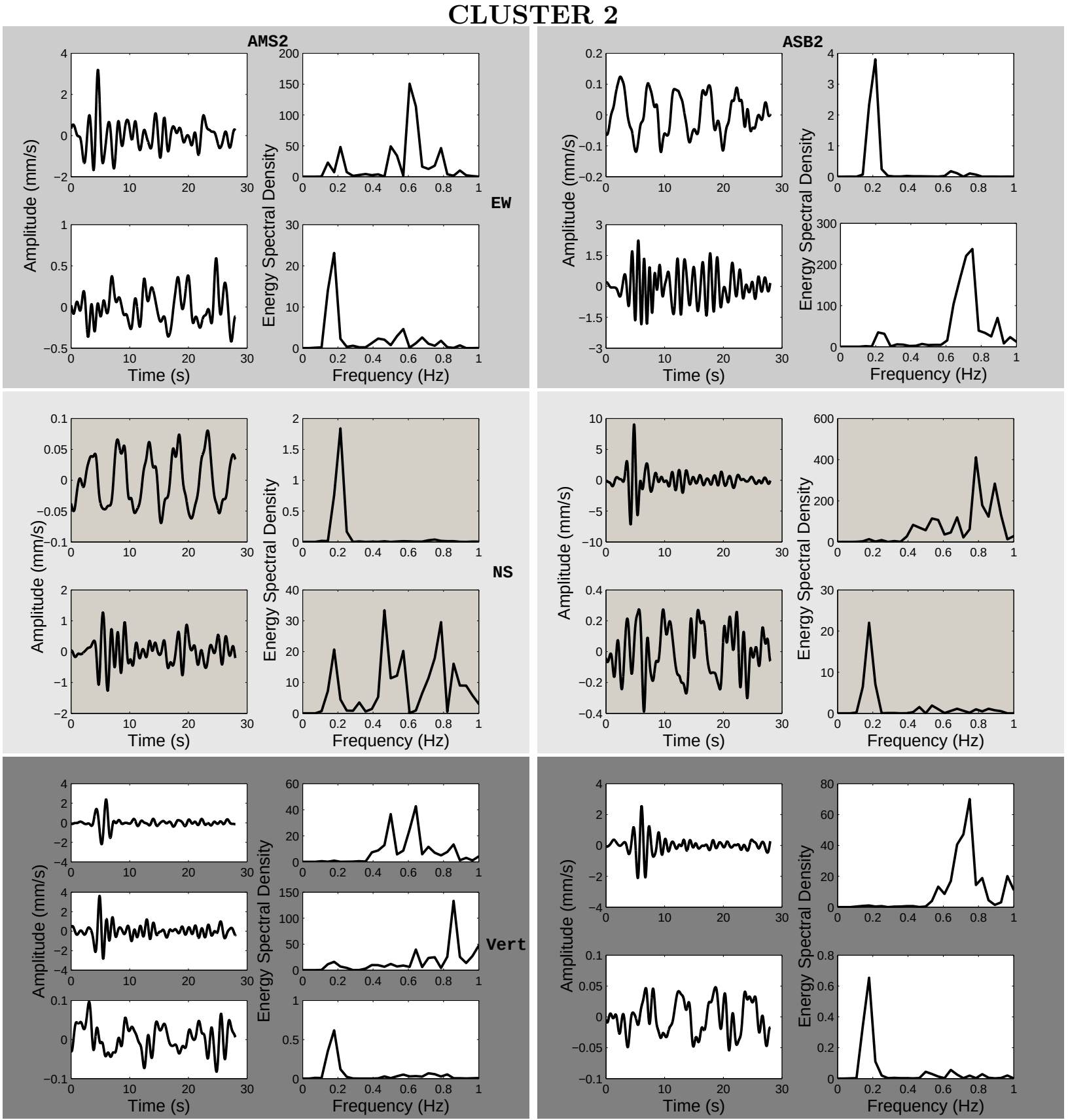

Figure(s)
Click here to download Figure(s): fig10.eps

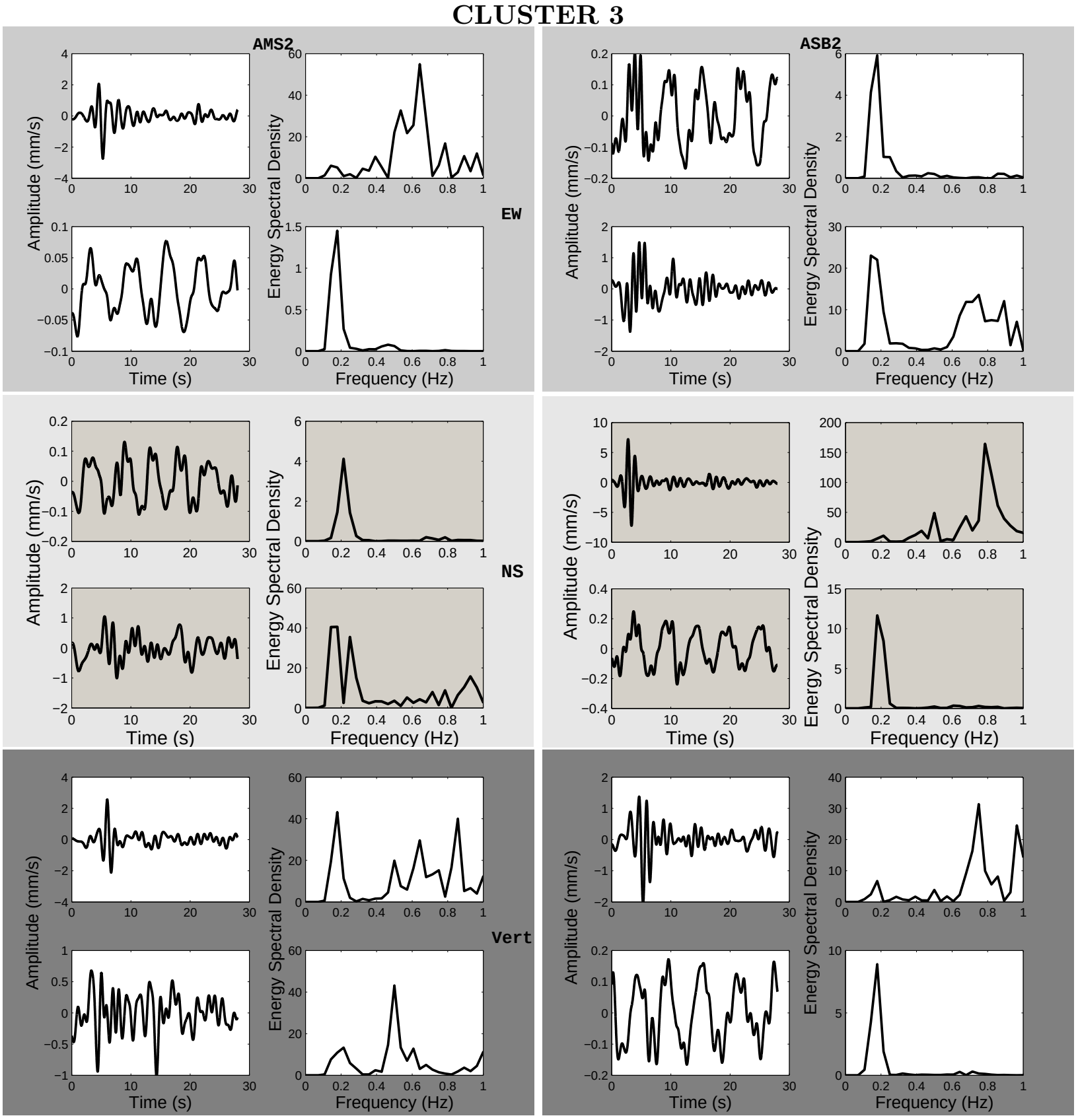

Figure(s)
Click here to download Figure(s): fig11.eps